

Research Article

doi.org/10.1002/prep.202100180

Effect of Me/B-Powder on the Ignition of High-Energy Materials

Alexander G. Korotkikh^{*[a, b]} and Ivan V. Sorokin^{*[a]}

Abstract: The study of the ignition characteristics of high-energy materials (HEMs) is important in solving a number of practical problems related to the assessment of explosion safety, the calculation of transition processes in power installation for various purposes (rocket and space technologies, weapons, pyrotechnics). This paper presents the experimental data on the thermal oxidation of ultrafine powder (UFP) based on Al/B, Ti/B, Ni/B, and Fe/B and the experimental characteristics of the ignition of HEM based on ammonium perchlorate, butadiene rubber, and metal fuel. In the course of processing thermal analysis data, the values of oxidation temperatures, the specific heat effect of the oxidation reaction, and the rate of weight gain of powder during heated at a constant rate of 10 °C/min in air

were determined. It was shown that the oxidation of Ti/B and Ni/B UFPs begins at temperature of 490–500 °C, which is 60–70 °C lower than the onset oxidation temperature for boron powder. The use of 15.7 wt.% the mixed UFP based on Al/B, Ti/B, Ni/B or Fe/B in HEM reduces the ignition delay time by 7–50% compared to boron-based HEM in the range of heat flux density from 60 to 200 W/cm². Based on experimental data of the ignition delay time versus the heat flux density, the formal activation energy, the multiplication of the specific heat flux of the reactions by the pre-exponent and the ignition temperature are calculated which could be used in mathematical modeling of the ignition for composite solid propellant containing metal fuels.

Keywords: High-energy material · Aluminum · Titanium · Nickel · Iron · Boron · Ignition temperature · Activation energy

1 Introduction

The main characteristics of high-energy materials (HEMs) of ignition and combustion (as applied to propulsion systems and engines) are the dependencies of the ignition delay time on the heat flux and the linear combustion rate on pressure, the ignition and combustion temperatures, the specific impulse of rocket engine, as well as the outflow rate, the chemical and particle size distribution of condensed combustion products. To improve the ignition and combustion characteristics of HEM, the combustion catalysts, powders of various metals or their oxides are used [1–6]. In order to increase the combustion heat and ignition characteristics of HEM, boron-based powders or metal borides are used. These powders have high value of the specific energy released during their oxidation [7–9]. However, the application of boron powder is complicated by the formation of an inert oxide layer on the particles surface, which leads to an increase in the ignition delay time and complete combustion time. To reduce the time and the temperature of boron ignition and to increase its combustion completeness, additives based on Mg, Al, Fe, Cu, Bi, Ce [10–14] are used, which make it possible to reduce the ignition times by up to two times [10], and the ignition temperature by 10% [11]. In addition, the introduction of such additives makes it possible to increase the completeness of conversion [10,11,13], which makes the use of bimetal

powder in HEM one of the most promising areas of research.

Research findings have been published on the study bimetal powder system characteristics [8,15] in which is noted that Al/B mixtures are characterized by short ignition time and lower ignition temperature in comparison with metal boride having the same phase composition. In their study [16,17] dedicated to oxidation, the ignition and combustion behaviors of boron-magnesium composites, authors note that the ignition temperature of the composition based on B/MgB₂ and the heat flux required for this have lower values than for a mixture of B/Mg or boron. In addition, the B/Mg mixture combusts faster than boron or B/MgB₂ composition in air-acetylene flame due to the rapid oxidation of elemental Mg in carbon dioxide.

Dossi and Maggi [18] studied the effect of mechanical activation of micrometric aluminum powder (30 µm) in order to increase its energetic characteristics. The activation of aluminum was carried out in a ball milling process with

[a] A. G. Korotkikh, I. V. Sorokin
National Research Tomsk Polytechnic University
Lenin Ave. 30, 634050 Tomsk, Russia
*e-mail: korotkikh@tpu.ru
ivans3485@gmail.com

[b] A. G. Korotkikh
National Research Tomsk State University
Lenin Ave. 36, 634050 Tomsk, Russia

and without additives of metal oxides. It was found that the activated materials have an irregular shape, and the content of the active metal decreases. The presence of 2.5% oxide additives causes a decrease in the content of active aluminum: by 3–4% for micron-sized additives (MoO_2 , PbO) and by 7% for nanometric ones (Fe_2O_3 , NiO). The TG/DTA data showed an increase in the reactivity of activated powders at both low and high heating rates. The authors note that activated aluminum without additives did not ignite during fast-heating tests, thus confirming the catalytic effect of the investigating metal oxides on the flammability and a decrease in the ignition temperature of aluminum.

The aim of the study is to improve the ignition characteristics and to determine the kinetic parameters of radiant ignition for HEM containing ammonium perchlorate (AP), butadiene rubber (BR), and a mixture of ultrafine powders (UFPs) based on various metals: aluminum, nickel, iron or titanium with boron, which can be used as energy-intensive metal fuel for composite solid and hybrid propellants.

2 Materials

We used a mechanical mixture of aluminum, titanium, nickel and iron UFPs with amorphous boron, in which the mass content of boron corresponded to the phase composition of the appropriate metal borides. The based metal UFPs were produced by the method of electric explosion of conductors in argon. According to manufacturing data (LLC "Advanced Powder Technologies", Russia), the mean diameter of the use metal powders was equal to from 70 to 110 nm. The values of the specific surface area of the particles S_{sp} and the content of active metal C_{ac} for the metal UFPs and boron are presented in Table 1.

The mixed Al/B, Ti/B, Ni/B, and Fe/B UFPs were prepared by mechanical mixing in a mass ratio, which corresponded

Table 1. The mean diameter, specific surface area and content of active metal of UFP.

Powder	d , nm	S_{sp} , m^2/g	C_{ac} , %
Al	90–110	15.5	90.0
Ni	70–80	6.0	99.8
Fe	90–110	7.7	92.0
Ti	80–110	13.8	93.8
B	210–240	8.6	99.5

Table 2. The mixed metal and boron UFPs.

Powder	Component content, wt. %	Metal boride phase
	Me	B
Al/B	55.5	AlB ₂
Ti/B	68.9	TiB ₂
Ni/B	84.5	NiB
Fe/B	83.8	FeB

to the phase composition of borides AlB₂, TiB₂, NiB, and FeB, per 10 g of the finished product (Figure 1), excluding the presence of oxide on the metal particle surface. To control the uniform distribution of particles in Me/B UFP, we used electron microscopy in combination with a silicon X-ray drift detector (EDS analyzer). The compositions of the investigated mixed Me/B UFPs are presented in Table 2.

We studied the HEM samples containing 64.6 wt. % bi-dispersed ammonium perchlorate (AP) (fractions with a particle size of less than 50 μm and 160–315 μm in the ratio of 40/60), 19.7 wt. % butadiene rubber (BR) plasticized by transformer oil, and 15.7 wt. % Me/B UFP specified in Table 2. In the study of ignition of the HEM samples, we used cured cylindrical samples 10 mm in diameter and 30 mm in height produced in a laboratory by extrusion pressing with subsequent curing.

3 Results and Discussion

3.1 Oxidation of Al/B, Ti/B, Ni/B and Fe/B UFPs

To study the reactivity of metal fuels, we used thermal analysis. Thermal analysis of boron and mixed metal with boron UFPs was carried out with a combined analyzer Netzsch STA 449 F3 Jupiter at a constant volumetric airflow. In the experiments, weighed portions of powders with a mass of ~5–8 mg were used, which were placed in ceramic crucibles (Al_2O_3) and then placed in a heating furnace. The metal with boron UFP was heated in a furnace from 30 to 1200 °C at a constant heating rate of 10 °C/min and an airflow rate of 150 ml/min.

The experimental data of the TG-DSC analysis for the investigated Me/B UFPs are shown in Figure 2. Based on the measured data, we determined the temperatures of the onset and intensive oxidation, the weight gain, the specific heat flux, and the oxidation rate for Me/B powders (Table 3). The temperature range with the maximum value of the oxidation rate of Me/B UFP was determined from the temperatures corresponding to 90% values of the maximum oxidation rate, i.e. at which the v_{ox} deviation did not exceed 10%.

The oxidation process for the amorphous boron and mixed Ti/B, Ni/B, and Fe/B UFPs is carried out in one stage in contrast to the Al/B UFP, which is characterized by a two-stage oxidation process, as for aluminum UFP [9]. Note that Al/B UFP has two main exothermic peaks with the maximum heat flux (21.5 and 43.9 W/g), separated by endothermic melting of aluminum at the temperature of ~660 °C. The first exothermic peak corresponds to the intense oxidation of aluminum nanoparticles due to the diffusion of the oxidant through the porous oxide layer and the phase transition of Al_2O_3 oxide. Therefore, the second peak (more significant) corresponds to the diffusion oxidation of aluminum and boron particles with intense heat release.

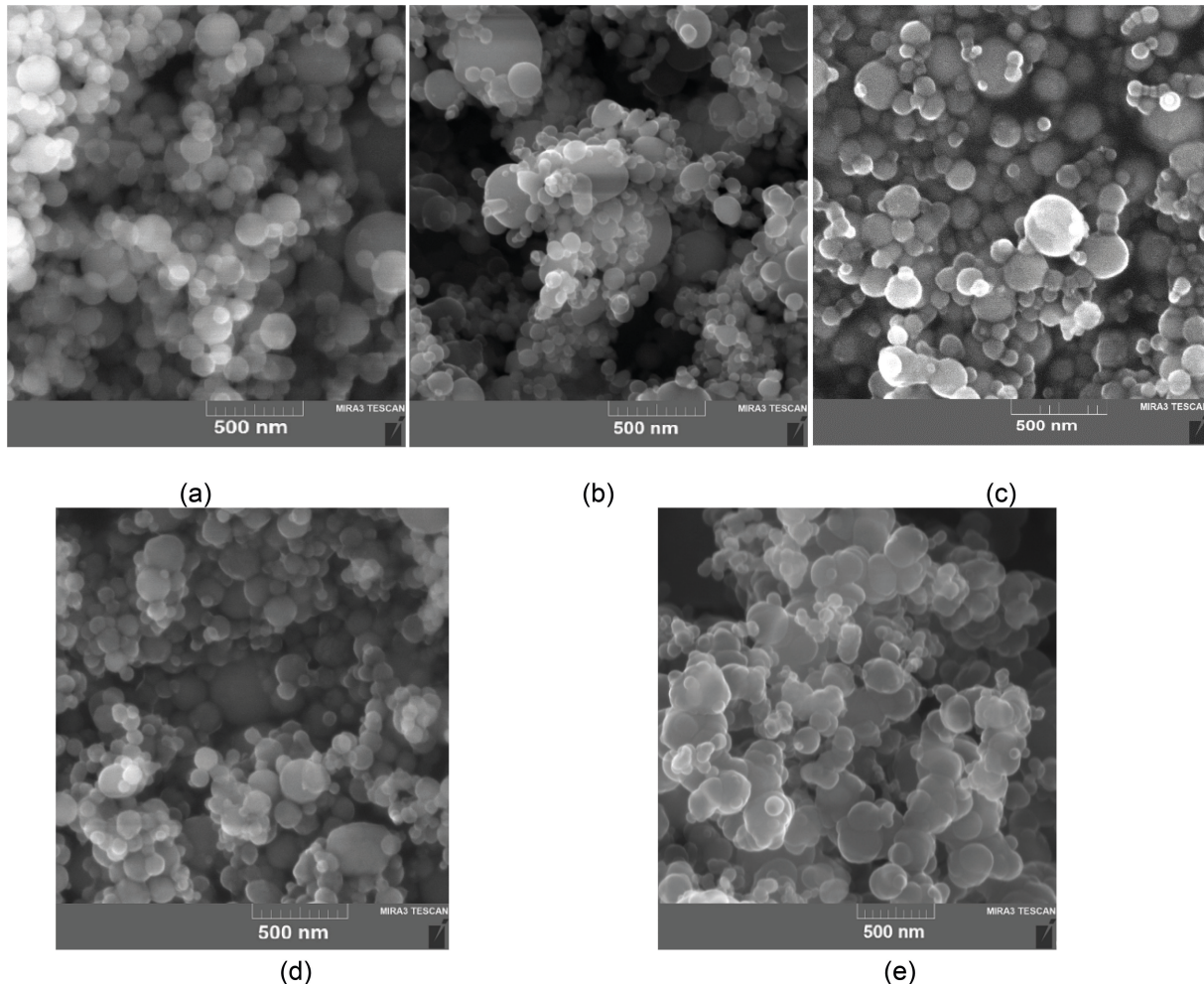


Figure 1. SEM images of aluminum (a), titanium (b), nickel (c), iron (d) and amorphous boron (e) UFPs.

Table 3. Oxidation temperature, specific oxidation heat, weight gain and maximum oxidation rate of boron, Me/B UFPs.

Powder	$T_{\text{on}}, ^\circ\text{C}$	$T_{\text{int}}, ^\circ\text{C}$	$T_{\text{end}}, ^\circ\text{C}$	$Q_s, \text{kJ/g}$	$\Delta m, \%$	$v_{\text{ox}}, \mu\text{g/s} (T, ^\circ\text{C})$
B	559	708	798	21.5	160	9.6 (655–735)
Al/B (55.5/44.5)	600	765	807	18.8	135	5.6 (745–770)
Ti/B (68.9/31.1)	498	564	635	12.7	98	6.2 (539–579)
Ni/B (84.5/15.5)	486	643	744	4.6	54	2.8 (625–645)
Fe/B (83.8/16.2)	179	593	643	11.6	56	5.2 (575–600)

Note: T_{on} is the onset temperature; T_{int} is the intensive temperature; T_{end} is the end temperature; Q_s is the specific oxidation heat; Δm is the weight gain; v_{ox} is the maximum oxidation rate.

The oxidation process of Ti/B and Ni/B UFPs begins at the temperature of 490–500 °C, which is 60–70 °C lower than T_{on} for boron powder. The onset oxidation temperature of Fe/B UFP is 179 °C. The low value T_{on} can be associated with the high reactivity of the UFP particles of iron and their pyrophoricity.

According to the data obtained by DSC analysis, the total specific heat release Q_s for boron powder is 21.5 kJ/g. The specific oxidation heat of Al/B UFP is 12.5% less than Q_s

for boron (Table 3). For Ti/B and Fe/B UFPs, the specific oxidation heats are 12.7 and 11.6 kJ/g, which is 1.7–1.9 times (or 41–46%) less than Q_s for boron. The minimum specific oxidation heat corresponds to Ni/B UFP and is 4.7 times (78%) lower than Q_s for boron.

The maximum oxidation rate for powders based on Al/B and Fe/B differ insignificantly and amount to 5.6 and 5.2 µg/s, respectively, while the indicated temperature range differs by ~170 °C (Table 3). The maximum oxidation

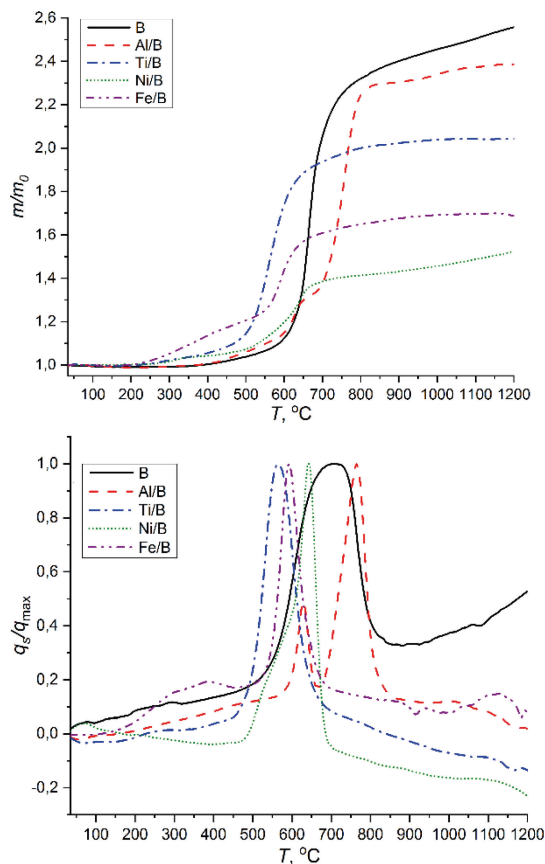


Figure 2. TG (a) and DSC (b) curves of Al/B, Ti/B, Ni/B and Fe/B mixed UFPS.

rate $v_{ox}=6.2 \mu\text{g/s}$ corresponds to Ti/B UFP, which indicates a high reactivity of titanium nanoparticles due to the presence of a passivating coating (hexane layer) on the particle surface, which is applied during the preparation of titanium powder.

3.2 Ignition Delay Time

The ignition characteristics of the HEM samples were determined on an experimental setup. The scheme and description of the experimental setup were presented in [14]. The setup includes a RLS-200 continuous CO₂ laser with a wavelength of 10.6 μm and maximum power of 200 W, power-supply unit, cooling system, and recording system of ignition characteristics. Prior to testing, the HEM sample was cut into tablets of 5 mm in height. The diameter of the laser beam at the exit from the semitransparent mirror of a CO₂ laser was approximately equal to the diameter of the sample. The ignition delay time t_{ign} of HEM was determined by the difference in the electrical signals of the photodiodes recording the initiation time of the sample (opening of the electromagnetic shutter) and the appearance of a glow flame on the end surface of the HEM sample. The heat

flux density was varied in the range from 60 to 210 W/cm² by changing the laser power, while the diameter of the laser beam was constant. The relative error in the measurement of the ignition delay time t_{ign} was equal to 5–10% with a confidence of 0.95.

We determined the ignition delay time of the HEM compositions containing boron and Me/B UFPs versus the heat flux density under radiant heating. Figure 3 depicts the measurement results as dots. The lines show the approximated dependences, which were used to determine the kinetic parameters of the HEM ignition.

The obtained experimental dependences were fitted to a power function of the following form:

$$t_{ign} = A \cdot q^{-B}, \quad (1)$$

where t_{ign} is the ignition delay time of the HEM sample, ms; q is the heat flux density, W/m²; A, B are fitted constants.

Fitted constants of the power-law dependence $t_{ign}(q)$ and R^2 determination coefficient for the experimental data are given in Table 4.

The experimental results of the ignition study depicted that using mechanical mixture of Me/B UFPs in the propellant composition reduces the ignition delay time in comparison with the boron-based HEM over the entire investi-

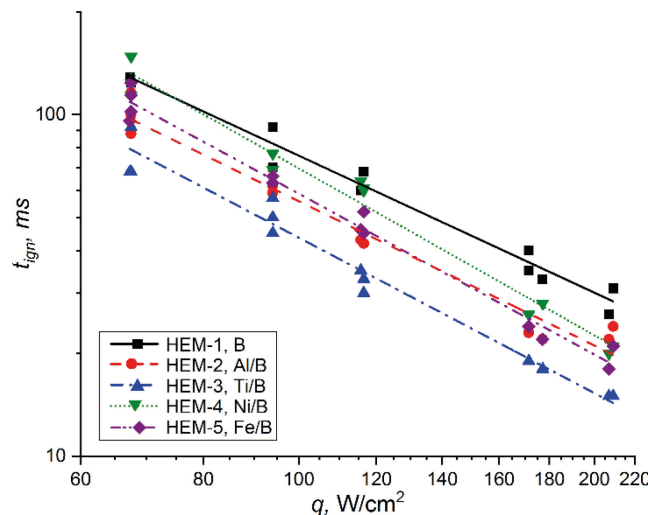


Figure 3. The ignition delay time of the HEM samples containing boron, Al/B, Ti/B, Ni/B, and Fe/B UFPs vs. the heat flux density.

Table 4. Fitted constants of Eq. (1) and determination coefficient.

HEM sample	A	B	R^2
HEM-1, B	$35.2 \cdot 10^3$	1.33 ± 0.08	0.97
HEM-2, Al/B	$35.8 \cdot 10^3$	1.40 ± 0.14	0.95
HEM-3, Ti/B	$46.1 \cdot 10^3$	1.51 ± 0.16	0.92
HEM-4, Ni/B	$123.9 \cdot 10^3$	1.63 ± 0.14	0.95
HEM-5, Fe/B	$79.3 \cdot 10^3$	1.57 ± 0.11	0.97

Table 5. Calculated kinetic parameters and ignition temperature of the HEM samples.

HEM sample	E , kJ/mol	$Q \cdot z$, W/g	T_{ign0} , K	T_{ign} , K at $q = 60\text{--}200$ W/cm 2	$T_{ign} - T_{ign0}$, K at $q = 60\text{--}200$ W/cm 2	q_{min} , W/cm 2
HEM-1, B	49	$2.85 \cdot 10^8$	507	519–630	12–123	51
HEM-2, Al/B	57	$5.26 \cdot 10^9$	477	490–575	13–98	48
HEM-3, Ti/B	73	$7.85 \cdot 10^{11}$	461	472–533	11–72	46
HEM-4, Ni/B	95	$1.66 \cdot 10^{13}$	521	526–585	5–64	54
HEM-5, Fe/B	81	$1.58 \cdot 10^{12}$	496	503–566	7–70	51

tigated range of heat flux density. The HEM-3 sample with Ti/B UFP has the greatest efficiency in reducing the ignition delay time t_{ign} (by 37–50%) and laser energy density (by ~40%) compared to HEM-1 with boron. The use of Al/B, Ni/B and Fe/B UFPs in the HEM composition reduces t_{ign} by 24–30, 7–27, and 13–36%, respectively, in comparison with the t_{ign} of the HEM-1. The use of metal/boron UFP in the HEM composition based on AP and BR promotes the intensification of the propellants component decomposition, increases the rate of chemical reactions, decreases the propellant ignition delay time and the delivered radiant energy density due to the high specific surface area and reactivity of ultrafine powder. It should be noted that the ignition delay time for the HEM-4 sample containing Ni/B UFP slightly differ from the t_{ign} value for HEM-1 with B at a heat flux density $q < 100$ W/cm 2 .

3.3 Activation Energy

To calculate the kinetic parameters of propellant ignition, we used the experimental dependences of the ignition delay time on the heat flux density. The formal activation energy, the reaction heat effect, the pre-exponential factor and the ignition temperature of the HEM samples were determined by the method presented in [19, 20]. It was assumed that all heat supplied through the end surface of the propellant sample is completely absorbed and there are no heat losses from the side surface of the sample. Heat transfer from the end surface is carried out deep into the sample along the laser beam symmetry axis. Heating the surface layer to the temperature T_{ign0} leads to the exothermic decomposition reactions of AP, BR and the oxidation onset of metal particles. The initial parameters in the calculation were the power-law dependences $t_{ign}(q)$ and the constant thermophysical parameters of HEM, which correspond to the solid propellant [14, 19]: density $\rho = 1.87$ g/cm 3 , specific thermal capacity $c = 1.24$ kJ/(kg K), thermal conductivity $\lambda = 0.66$ W/(m K). Table 5 shows the calculated data of the kinetic parameters and ignition temperature of the studied HEM samples.

According to the calculated data, the highest value of the activation energy ($E = 95$ kJ/mol), the multiplication of the specific heat flux of the reactions by the pre-exponent ($Q \cdot z = 1.66 \cdot 10^{13}$ W/g), and the ignition temperature ($T_{ign} =$

526 K at $q = 65$ W/cm 2) were obtained for the HEM-4 sample containing a mixture of Ni/B, which has the maximum heating and ignition times. The HEM-1 sample with boron has the minimum activation energy E and $Q \cdot z$ multiplication (49 kJ/mol and $2.85 \cdot 10^8$ W/g). However, the temperature on the surface of the reaction layer T_{ign} at the time of the incandescence appearance is higher than for HEMs containing Al/B, Ti/B, Ni/B and Fe/B UFPs. With an increase in the heat flux density from 60 to 200 W/cm 2 , the temperature T_{ign} on the HEM surface increases by 59–63 K for the HEM samples with Ti/B, Ni/B, Fe/B UFPs and by 85, 111 K for the HEM with Al/B and B UFPs.

3.4 Ignition Temperature

During the radiant heating and ignition of the HEM sample, we measured the temperature field on the surface of the HEMs containing Me/B UFPs at a constant $q = 68$ W/cm 2 . We used Jade J530 SB thermal imaging camera, which records temperatures at a high frame rate (20 ms interval between frames). The dependence of the maximum surface temperature T_{ign} on the heating time of the HEM was plotted in the Altair software package (Figure 4). Table 6 shows the temperature values on the HEM sample surface, corresponding to the time t_{ign} and the appearance of the flame glow. After

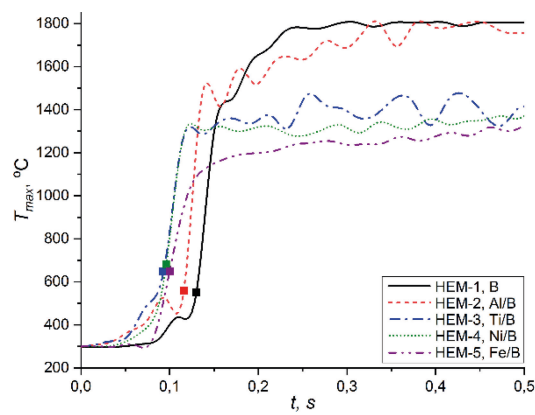


Figure 4. Surface temperature vs. heating time for the HEM samples containing B, Al/B, Ti/B, Ni/B, and Fe/B UFPs (the points correspond to the values of the ignition time).

Table 6. Measured ignition temperature and maximum flame front length of the HEM samples.

HEM sample	T_{ign} , °C	l_{max} mm
HEM-1, B	550 ± 50	165 ± 5
HEM-2, Al/B	560 ± 30	245 ± 5
HEM-3, Ti/B	650 ± 40	270 ± 5
HEM-4, Ni/B	680 ± 60	270 ± 5
HEM-5, Fe/B	650 ± 50	300 ± 5

that, the flame front spreads over the end surface of the HEM sample and increases in the axial direction. The measured ignition temperatures for the HEM-3 with Ti/B, HEM-4 with Ni/B and HEM-5 with Fe/B are 650–680 °C, which is 100–130 °C higher in comparison with HEM-1 with B or HEM-2 with Al/B (Table 6). Higher ignition temperature on the surface of the HEM-3, HEM-4, HEM-5 samples is due to low onset and intense oxidation temperatures of Ti/B, Ni/B and Fe/B UFPs (see Table 3), which add additional heat during their oxidation in the reaction layer of sample.

Depending on the component composition of the HEM, the unsteady mode of propellant ignition goes over to the steady mode of combustion after 120–220 ms. Thus, this mode is accompanied by a sharp increase in temperature on the reaction layer surface of propellant and the outflow rate of gasification products with metal and boron nanoparticles from the end surface due to intense heat release in the reaction zone of condensed phase and radiant heat transfer on the sample surface. The flow rate of gas products during the ignition period is determined by the reactivity and reaction rate of the HEM components.

Figure 5 depicts high-speed video recording frames of the ignition stages and subsequent combustion for HEMs containing Me/B UFP at the heating by a radiant flux $q = 68 \text{ W/cm}^2$. The processing of the frames made it possible to determine the maximum length l_{max} of the HEM flame front (Table 6) and highlight the main features of the propellant ignition stages. The length l_{max} above the end surface of sample corresponds to the transition to stationary combustion of the HEM. During heating of the HEM surface from the initial temperature to T_{ign} , an incandescence is formed on the end surface in the area of the maximum heat flux of the laser beam (local focus), the value of which is described by Gaussian distribution. The sample surface is heated in the surrounding area of local focus, but with a lower temperature gradient and conductive heat transfer. For the HEM samples containing Ti/B, Ni/B and Fe/B UFP, the period of heating and ignition is ~100 ms, which is explained by the high reactivity of Ti, Ni and Fe UFPs. The appearance of an incandescence or a flash in the local heating area intensifies the supply of heat to the propellant surface and increases the flame zone in the axial and radial directions. The time of visible flame formation on the HEM surface is 17–26 ms. Thus, there is a sharp rise in temperature on the surface of the reaction propellant layer. An increase in the

temperature on the propellant surface is associated with the intensification of heat supply from the gas-phase zone of chemical reactions and heat transfer due to convection and radiation, as well as additional heat release during the ignition of metal fuel particles. The maximum length of the flame front for the HEMs containing Ti/B, Ni/B and Fe/B UFPs is in the range of 270–300 mm. The high activity of metal nanoparticles, fragmentation of titanium particles, and the catalytic interaction of iron and nickel oxides with AP crystals in the reaction layer of the sample increases the rate of outflow of decomposition products from the sample surface, and also reduces the formation time of a visible flame and the ignition time of boron particles, which increases the heat flux to the condensed phase of HEM.

4 Conclusion

We studied the thermal oxidation characteristics of the ultrafine powders based on B, Al/B, Ti/B, Ni/B and Fe/B and their effect on ignition characteristics (ignition delays time, ignition temperature and activation energy) of the HEM samples containing AP and butadiene rubber.

Data of TG and DSC analysis in airflow showed that Ti/B, Ni/B and Fe/B UFPs have lower values of the onset and intense oxidation temperature, specific oxidation heat and the rate of weight gain in comparison with boron UFP. The intense oxidation temperatures of the Ti/B and Fe/B UFPs are 564 and 593 °C, and lower than boron or Al/B UFP, while their maximum oxidation rates are 6.2 and 5.2 $\mu\text{g/s}$, respectively.

The use of Me/B UFPs as part of the HEM leads to a decrease in the propellant ignition delay time by 7–50% in comparison with the boron-based HEM. The most effective HEM are compositions with Ti/B, Ni/B and Fe/B UFPs, which decrease the ignition delay time of propellant and the energy density from a radiation source. Moreover, these HEM compositions increase temperature on the surface of the reaction layer and the length of the flame front by 18–24 and 64–82%, respectively.

Symbols and Abbreviations

A, B	Fitted constants
C_{ac}	Content of active metal
c	Specific thermal capacity
d	Mean diameter
E	Activation energy
l_{max}	Maximum length of the flame front
Q	Specific heat flux of the chemical reactions
Q_s	Specific oxidation heat
q	Heat flux density
R^2	Determination coefficient
S_{sp}	Specific surface area
T_{end}	End temperature

Effect of Me/B-Powder on the Ignition of High-Energy Materials



Figure 5. Video recording frames of ignition of the HEM samples containing boron and Me/B UFPs at $q=68 \text{ W/cm}^2$.

T_{ign}	Ignition temperature
t_{ign}	Ignition delay time
T_{int}	Intensive temperature
T_{on}	Onset temperature
V_{ox}	Maximum oxidation rate
z	Pre-exponential factor
Δm	Weight gain
λ	Thermal conductivity
ρ	Density
AP	Ammonium perchlorate
BR	Butadiene rubber
DSC	Differential Scanning Calorimetry
EDS	Energy dispersive spectroscopy
HEM	High-energy material
SEM	Scanning electron microscope
TG	Thermogravimetry
UFP	Ultrafine powder

Acknowledgements

The reported study was supported by RFBR according to the research project No. 20-03-00588.

Data Availability Statement

The data that support the findings of this study are available from the corresponding author upon reasonable request.

References

- [1] Sh. L. Huseynov, S. G. Fedorov, Nanopowders of aluminum, boron, aluminum and silicon borides in high-energy materials, Torus Press, Moscow 2015, p. 255.
- [2] V. P. Sinditskii, A. N. Chernyi, Sw. Kyaw, R. S. Bobylev, Combustion of the mixture of ammonium perchlorate with high-calorific fuels, *Uspekhi v khimii i khimicheskoy tekhnologii* 2016, 30, 18–20.
- [3] A. G. Korotkikh, O. G. Glotov, V. A. Arkhipov, V. E. Zarko, A. B. Kiskin, Effect of iron and boron ultrafine powders on combustion of aluminized solid propellants, *Combust. Flame* 2017, 178, 195–204.
- [4] A. V. Sergienko, E. P. Popenko, K. V. Slyusarsky, K. B. Larionov, E. L. Dzidziguri, E. S. Kondratyeva, A. A. Gromov, Burning characteristics of the HMX/CL-20/AP/polyvinyltetrazole binder/Al solid propellants loaded with nanometals, *Propellants Explos. Pyrotech.* 2019, 44, 217–223.
- [5] L. Gong, J. Li, Y. Li, R. Yang, Combustion properties of composite propellants based on two kinds of polyether binders and different oxidizers, *Propellants Explos. Pyrotech.* 2020, 45, 1634–1644.
- [6] Y. Li, W. Xie, H. Wang, H. Yang, H. Huang, Y. Liu, X. Fan, Investigation on the thermal behavior of ammonium dinitramide with different copper-based catalysts, *Propellants Explos. Pyrotech.* 2020, 45, 1607–1613.
- [7] A. G. Korotkikh, V. A. Arkhipov, K. V. Slyusarsky, I. V. Sorokin, Study of ignition of high-energy materials with boron and aluminum and titanium diborides, *Combust. Explos. Shock Waves* 2018, 54, 350–356.
- [8] F. K. Bulanin, A. E. Sidorov, S. A. Kiro, N. I. Poletaev, V. G. Shevchuk, Ignition of metal boride particle-air mixtures, *Combust. Explos. Shock Waves* 2020, 56, 57–62.
- [9] A. G. Korotkikh, I. V. Sorokin, Study of the chemical activity of metal powders based on aluminum, boron and titanium, *AIP Conf. Proc.* 2020, 2212, 020029-1–020029-6.
- [10] J. Xi, J. Liu, Y. Wang, Y. Hu, Y. Zhang, J. Zhou, Metal oxides as catalysts for boron oxidation, *J. Propul. Power* 2014, 30, 47–53.
- [11] J.-Z. Liu, J.-F. Xi, W.-J. Yang, Y.-R. Hu, Y.-W. Zhang, Y. Wang, J.-H. Zhou, Effect of magnesium on the burning characteristics of boron particles, *Acta Astronaut.* 2014, 96, 89–96.
- [12] S. Xu, Yu. Chen, X. Chen, D. Wu, D. Liu, Combustion heat of the Al/B powder and its application in metallized explosives in underwater explosions, *Fiz. Gorenija Vzryva* 2016, 52, 97–104.
- [13] L.-J. Liu, G.-Q. He, Y.-H. Wang, Thermal reaction characteristics of the boron used in the fuel-rich propellant, *J. Therm. Anal. Calorim.* 2012, 114, 1057–1068.
- [14] A. G. Korotkikh, I. V. Sorokin, E. A. Selikhova, V. A. Arkhipov, Effect of B, Fe, Ti, Cu nanopowders on the laser ignition of Al-based high-energy materials, *Combust. Flame* 2020, 222, 103–110.
- [15] D. Liang, R. Xiao, J. Liu, Y. Wang, Ignition and heterogeneous combustion of aluminum boride and boron-aluminum blend, *Aerosol Sci. Technol.* 2019, 84, 1081–1091.
- [16] Y. Sun, H. Ren, Q. Jiao, M. Schoenitz, E. L. Dreizin, Oxidation, ignition and combustion behaviors of differently prepared boron-magnesium composites, *Combust. Flame* 2020, 221, 11–19.
- [17] Y. Sun, H. Ren, Q. Jiao, Y. Li, H. Xu, X. Yu, W. Zhang, Q. Lu, Ignition and combustion behavior of sintered-B/MgB₂ combined with KNO₃, *Propellants Explos. Pyrotech.* 2020, 45, 997–1004.
- [18] S. Dossi, F. Maggi, Ignition of mechanically activated aluminum powders doped with metal oxides, *Propellants Explos. Pyrotech.* 2019, 44, 1312–1318.
- [19] V. E. Zarko, A. G. Knyazeva, Determination of kinetic parameters of exothermic condensed phase reaction using the energetic material ignition delay data, *Combust. Flame* 2020, 221, 453–461.
- [20] A. G. Korotkikh, I. V. Sorokin, E. A. Selikhova, V. A. Arkhipov, Ignition and Combustion of Composite Solid Propellants Based on a Double Oxidizer and Boron-Based Additives, *Russ. J. Phys. Chem. B* 2020, 14, 592–600.

Manuscript received: June 17, 2021
Revised manuscript received: August 15, 2021
Version of record online: September 27, 2021